First Plasmas in Heliotron J

T. Obiki 1), T. Mizuuchi 1), K. Nagasaki 1), H. Okada 1), S. Besshou 2), F. Sano 1), K. Kondo 2), Y. Liu 1)*, Y. Nakamura 2), K. Hanatani 1), M. Nakasuga 2), M. Wakatani 2), T. Hamada 1), Y. Manabe 1), H. Shidara 1), O. Yamagishi 2), K. Aizawa 2), W. L. Ang 1), Y. Ikeda 1), Y. Kawazome 2), T. Kobayashi 1), S. Maeno 2), T. Takamiya 1), M. Takeda 1), K. Tomiyama 2), Y. Ijiri 1), T. Senju 1), K. Yaguchi 1), K. Sakamoto 1), K. Toshi 1), M. Shibano 1)

1) Institute of Advanced Energy, Kyoto University, Gokasho, Uji 611-0011, Japan.
2) Graduate School of Energy Science, Kyoto University, Gokasho, Uji 611-0011, Japan.

e-mail contact of main author: obiki@iae.kyoto-u.ac.jp

Abstract Results obtained in the initial experimental phase of Heliotron J are reported. The electron beam mapping of the magnetic surfaces has revealed that the observed surfaces are in basic agreement with the calculated ones based on the measured ambient field around the device. For 53.2-GHz second harmonic ECH hydrogen plasmas, a fairly wide resonance range for breakdown by the TE_{02} mode has been observed in Heliotron J as compared with that of Heliotron E. With ECH injection powers up to ~ 400 kW, diamagnetic stored energies up to ~ 0.7 kJ were obtained without the optimized density control.

1. Introduction

Heliotron J is a medium-sized plasma device that is designed and constructed to be a first step on the way toward the optimized helical-axis heliotron. In association with the planar axis heliotron, e.g., Heliotron E and LHD, the helical-axis heliotron studies can open up a new frontier of the plasma confinement in terms of its beneficial effects caused by the helical axis [1, 2]. Moreover, the heliotrons with continuous helical-coils and the advanced stellarators with modular coils, e.g., W7-AS and HSX constitute complementary approaches to develop the physics and engineering understanding of the helical system. The optimal tradeoff among the simplicity of coil design, neoclassical transport, MHD and divertors forms interesting physics studies that stimulate us to develop a new concept-exploration device in the heliotron line. From this viewpoint, the goals of the Heliotron J experiments are (1) to explore the non-symmetric, quasi-isodynamic optimization concept for the helical-axis heliotron configuration, (2) to establish the design principle for the proof-of-principle facility based on this concept and (3) to understand the physics that is specific to the helical-axis heliotron [3, 4]. The experimental program is organized to study the high-level compatibility between good particle confinement and MHD stability as well as its divertor scheme. The concept-exploration experiments of the island divertor can also be made together with that of the helical divertor [5].

Photograph and schematic of the device are shown in FIG. 1. The coil system is composed of an L=1/M=4 continuous helical coil (HFC), two types of toroidal coils (TFC-A and -B) and three pairs of vertical coils (MVFC, IVFC and AVFC) [6]. Here L is the pole number of the helical coil and M is the pitch number of the field along the torus. The device parameters are listed in TAB. I. The two types of the discharge cleaning methods were prepared; 2.45-GHz ECH discharge and glow discharge. The latter was mainly employed with H_2 gas in the first experimental phase. A titanium getter was also applied for the PSI control.

Among a wide variety of the helical-axis heliotron configurations, the configuration with an aspect ratio of $A \sim 7$ is selected for the basic configuration (BSC) of Heliotron J since it could combine attractive features of good particle confinement and edge magnetic well. This

---

* Permanent Address: Southwestern Institute of Physics, Chengdu, 610041, China

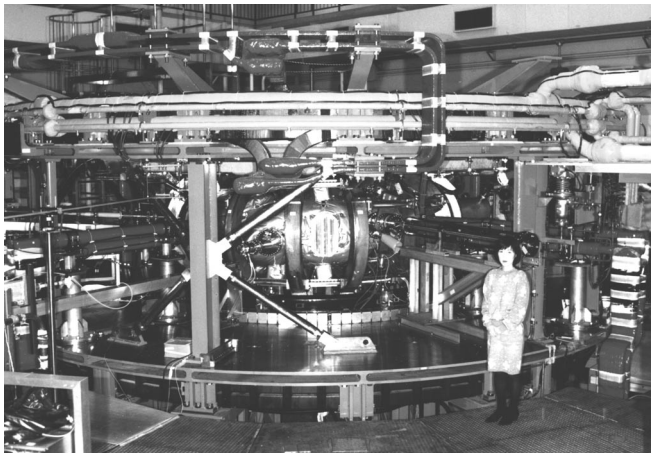

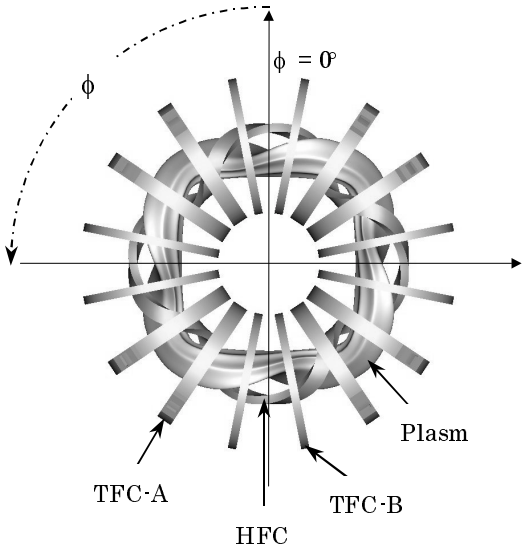

FIG.1 Photograph of the Heliotron J device (Left). Schematic top view of HFC, TFCs and plasma (Right).

TAB.I Device Parameters of Heliotron J

Major Plasma Radius, R	1.2 m
Average Plasma Minor Radius, $\langle a_p \rangle$	0.1–0.2 m
Inside Surface Area of the Vacuum Chamber	~ 15 m^2
Magnetic Field Strength, B (on the magnetic axis)	≤ 1.5 T
Vacuum Rotational Transform, $\iota/2\pi$	0.3–0.8 with low magnetic shear
Magnetic Well Depth	1.5 % at the plasma edge
Flat-Top Time of the Field	0.5 s
Heating Systems	ECH: 0.5 MW NBI: 1.5 MW ICRF: 2.5 MW

configuration can constitute the local isodynamic configuration in the straight section of the confinement field [2]. In this configuration, the Mercier mode is stable up to the equilibrium β-limit. According to the ballooning quasi-mode analysis, it is suspected that toroidally localized ballooning mode can be unstable at $\beta_{axis} > 0.5\%$. In order to clarify the stability β-limit against the ballooning mode, however, the global mode analysis will be necessary. The BSC configuration is realized only by the basic coils of the device, i.e. HFC, MVFC and TFCs. By imposing additional AV and IV fields to this configuration, the distance can be increased between the wall and the last closed magnetic surface (LCMS) with maintaining almost all the favorable features of core confinement. This is a standard configuration with a helical divertor in Heliotron J (STD) [5]. In this paper, we report the initial experimental results in these two configurations.

2. Measurement of the Vacuum Magnetic Surfaces

The first examination of the vacuum magnetic surfaces in Heliotron J was performed by using a directed low energy electron beam ($V_{acc} \leq 100$ eV, $I_{beam} \sim 10$ μA, $r_{beam} \sim 0.25$ mm) in combination with a movable fluorescent rod at a reduced DC magnetic field of ~ 0.03 T. The gun was inserted from the top at $\phi = 0°$. The beam position was detected by scanning the rod at $\phi = 67.5°$. The perspective fluorescence images taken with a CCD camera were converted to the corrected images by using the scale markers.

The corrected image for the STD configuration is shown in FIG. 2(a). Due to the low field experiment, we must take into account the ambient “error” field caused by the terrestrial magnetism and the residual fields from magnetized materials around the device. The ambient

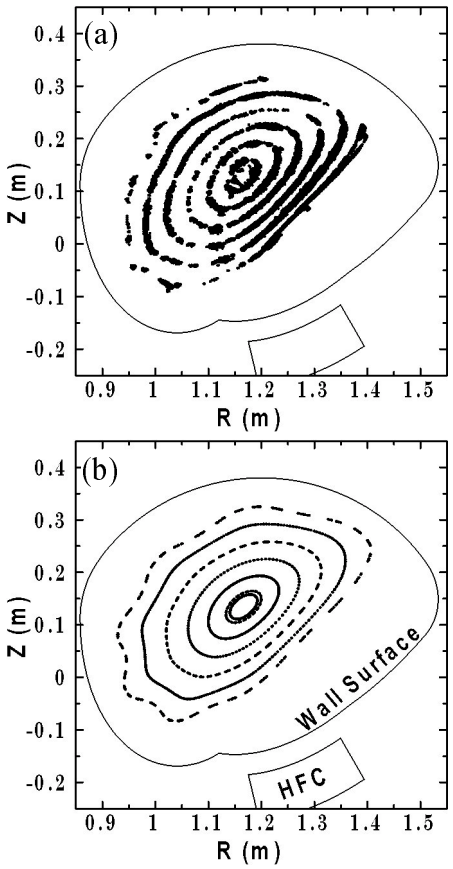

FIG. 2 The magnetic surfaces at ϕ = 67.5° in the STD configuration. (a) The corrected image. (b) The calculated magnetic surfaces.

field was measured without the coil excitation. Although the distribution of the measured field was complicated, the largest component was the downward one of ~ 1.5×10^{-4} T. The calculated magnetic surfaces with the lowest mode of the "error" components are shown in FIG. 2(b), where the setting inaccuracy of the coil currents is also considered. The calculated surfaces are in basic agreement with the measured ones. In the BSC configuration, the basic agreement is also observed but some minor differences remain in some inner surfaces. The effects of the higher modes in the ambient field, which are neglected in the above calculation, might become noticeable in these cases.

It should be noted that the substantial agreement between the measured and calculated surfaces is obtained without any distortion of the coil alignment in both cases. Thus, we can conclude that the present coil setting does not raise any serious problem to produce the expected confinement surfaces. However, since the $\iota/2\pi$ of these configurations is off resonant from low mode error fields, their effects on the surface topology near the resonant condition are still an open question. According to the calculation based on a simple model of the current path distortion at the HFC feeders, it is indicated that the existence of the m/n=2/1 error field cannot be excluded. Since the configurations with $\iota/2\pi \sim 0.5$ are attractive for the island divertor study [7], we must experimentally check the soundness of that field topology to realize the island divertor.

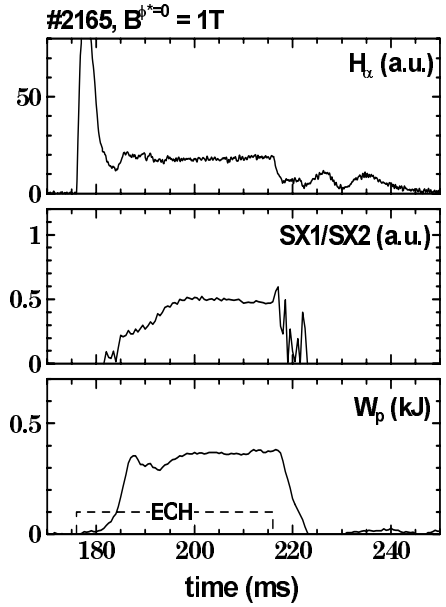

FIG. 3 Time trace of ECH plasma at the STD configuration. Hα intensity (Top), ratio of two filtered SX-signal (Middle) and diamagnetic stored energy (Bottom).

3. ECH Plasmas

Current-free plasmas have been successfully produced by the second harmonic ECH (53.2 GHz, $P_{ECH} \leq 400$ kW, $\Delta t \sim 50$ ms). The TE_{02} mode waves generated by three gyrotrons were injected through smoothed oversized waveguides (two gyrotrons are at $\phi \approx 129°$ and one is at $\phi \approx 203°$). A time trace of ECH plasma is shown in FIG. 3.

To investigate the plasma production window under the fixed configuration, the B-dependence of the plasma breakdown was examined under the fixed gas-puffing condition. The initial peak intensity of H_α signal and its delay time after the ECH turn-on are plotted as a measure of the plasma production in FIG. 4 for the BSC case. The plasma is produced in a wide range, $0.40 \leq \omega_0/\omega \leq 0.75$ ($0.8\ T < B^{\phi^*=0°} < 1.4\ T$) Here ω_0 is the electron cyclotron frequency for the magnetic field strength on the axis, $B^{\phi^*=0°}$ is the magnetic field at $\phi^* = 0°$ (ϕ^*: the toroidal angle in a field pitch.) and ω is the frequency of the microwaves. The plasma starts up fast when the magnetic

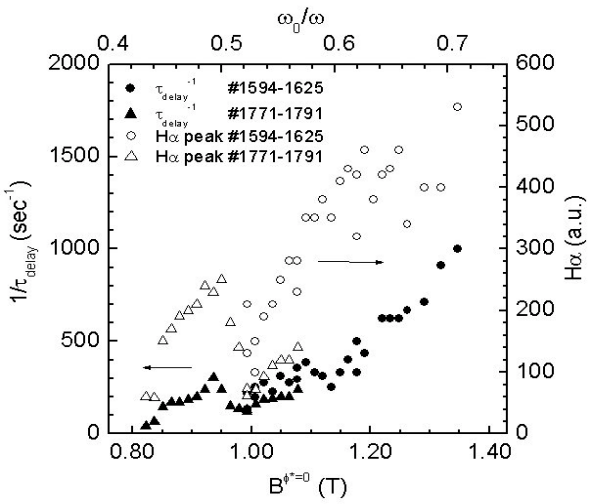

FIG. 4 Dependence of plasma breakdown on magnetic field strength in the BSC configuration.

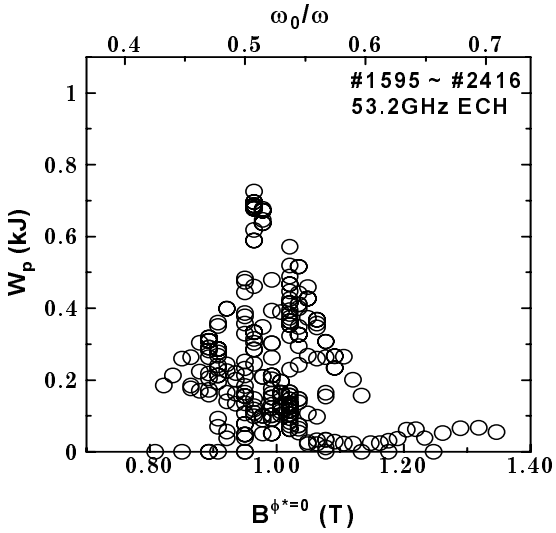

FIG. 5 Dependence of the diamagnetic stored energy on the magnetic field strength.

field is $\omega_0/\omega \approx 0.48$–$0.5$. This condition corresponds to the situation where the resonance layer is close to the magnetic axis. For $\omega_0/\omega < 0.50$, the plasma first appears around the magnetic axis in the snake-like form, and then expands to the whole confinement region. This snake-like plasma is not seen for $\omega_0/\omega > 0.51$. When the magnetic field is larger, i.e., $\omega_0/\omega > 0.52$, the plasma start-up becomes faster with B in spite of the outward shift of the resonance layer. The same tendencies were also observed in the STD configuration. The fundamental resonance appears within the LCMS only when ω_0/ω is larger than ~ 0.61 for the BSC case. This may indicate that the fundamental resonance contributes to the plasma initiation even when it is located outside the LCMS. This contrasts with the B-dependence in Heliotron E [8], where the B-region for plasma production is discrete at the fundamental and second harmonic ECH, and the fundamental resonance does not work for the plasma initiation if it shifts outside the LCMS.

The operational magnetic field window for the efficient second harmonic heating is compressed into a narrower range from that for the plasma production. Figure 5 shows the stored energy W_p measured with a diamagnetic loop as a function of the magnetic field strength. Here, all the data obtained during this experimental period ($P_{ECH} \approx 100$–400 kW) are plotted. Although the density control was not optimized yet, the value of $W_p \approx 0.7$ kJ was obtained, which corresponds to $\langle\beta\rangle \sim 0.2$ %. The VUV spectra show the existence of metal impurities such as Fe and Ti besides light impurities (C and O). The level of the total radiation loss estimated from the bolometers is less than ~ 20 % of the input power. The observed VUV spectra indicate that the plasma of $T_e \geq$ 300-400 eV was created, while the accurate temperature measurements are now in preparation.

The edge plasma properties were monitored by using three Langmuir probe sets: one is a movable array (SOL-probe) at $\phi = 247.5°$ (outward, $\phi^* = 67.5°$) and the others are fixed probe arrays near the wall (Div-probe) at $\phi = 67.5°$ (top) and 112.5° (bottom). For the STD case, the position of the Div-probes is close to one apex of the LCMS. The SOL-probe scans the region between the apexes radially. An example of T_e^{SOL}-, n_e^{SOL}- and V_f^{SOL}-distributions for a typical ECH discharge ($P_{ECH} \approx 250$ kW) in the STD configuration is plotted in FIG. 6 as a function of the distance to the LCMS. The values near the LCMS are $T_e^{SOL} \approx$ 40-50 eV, $n_e^{SOL} \approx 1$–2×10^{18} m^{-3} and $V_f^{SOL} \approx 60$–70 V, respectively. The SOL density exponentially decays with

the distance to the LCMS. The SOL width (the e-holding length) for n_e^{SOL} is about ~ 4 cm. Although the temperature gradient seems to become low near the LCMS, T_e^{SOL} shows almost the same dependence as n_e^{SOL} in the region far from the LCMS. The electron temperature measured with the Div-probes is almost the same as that from the SOL-probe (FIG. 6). The densities from both probes agree within a factor of two.

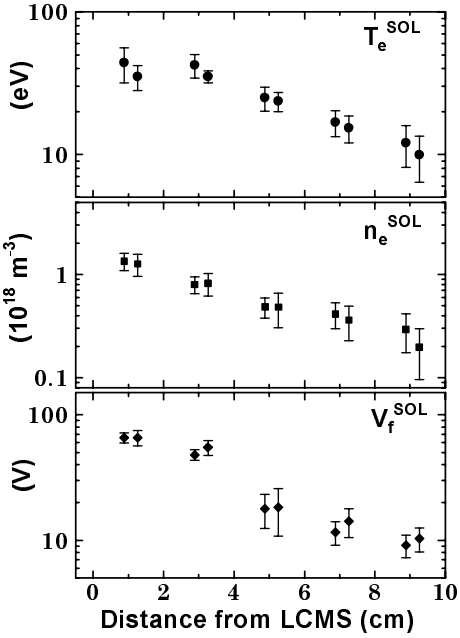

FIG. 6 T_e^{SOL}-, n^{SOL}- and V_f^{SOL}-distributions in the SOL region for the ECH plasmas as a function of the distance to the LCMS.

4. Summary

The confinement experiments of the helical-axis heliotron plasma in Heliotron J have begun to explore the design principles for the quasi-isodynamic optimization approach to the heliotron line. The measurements of the magnetic flux surfaces have revealed the soundness of the coil setting. The initial plasma experiments have shown that the formation of high temperature plasmas adequate for the detailed confinement studies can be obtained with 200–400 kW of the second harmonic ECH at ~ 1 T with the low-shear magnetic flux surfaces. The observed wide range for plasma production may be explained from the unique field structure of this device.

Attempts to improve the confinement performance are being carried out. Near-term plans are as follows:

1) The intensive PSI control to expand the operation regime with regard to impurities and recycling.
2) The configuration control with regard to bumpiness, magnetic well, and helical/island divertors.
3) The upgrade/installation of the heating systems such as 70 GHz, 500 kW ECH system and ICRF system.

Acknowledgements

The authors acknowledge Dr. M. Yokoyama for valuable discussions. This work was partially supported by the Collaboration Program of the Laboratory for Complex Energy Processes, Institute of Advanced Energy of Kyoto University.

References

[1] OBIKI, T., et al., Nucl. Fusion 39 (1999) 1667.
[2] WAKATANI, M., Nucl. Fusion 40 (2000) 569.
[3] SANO, F., et al., J. Plasma Fusion Res. SERIES 1(1998)168.
[4] OBIKI, T., et al., Proc.12th International Stellarator Workshop (Madison, USA, 1999).
[5] MIZUUCHI, T., et al., ibid.
[6] SANO, F., et al., ibid.
[7] MIZUUCHI, T., et al., 19th PSI Conf. (Rosenheim, Germany, 2000). .
[8] IIYOSHI, A., et al., Proc. 10th Int. Conf. on Plasma Physics and Controlled Nuclear Fusion Research, 1984 London (IAEA, Vienna, 1985) Vol. 1, 453.